PAPER • OPEN ACCESS

Temperature dependent pinning efficiency in multilayer and single layer BZO/YBCO nanocomposite films

To cite this article: M Panth et al 2022 IOP Conf. Ser.: Mater. Sci. Eng. 1241 012021

View the article online for updates and enhancements.

You may also like

- High critical current density over 1 MA cm² at 13 T in BaZrO₃ incorporated Ba(Fe,Co)₂As₂ thin film Jongmin Lee, Jianyi Jiang, Fumitake Kametani et al.
- New insight into strain and composition of BaZrO₃ nanorods in REBCO superconductor Goran Majkic, Jong Seok Jeong, Hwanhui Yun et al
- Enabling coherent BaZrO₃
 nanorods/YBa₂Cu₃O_{7x} interface through dynamic lattice enlargement in vertical epitaxy of BaZrO₃/YBa₂Cu₃O_{7x}
 nanocomposites
 Judy Z Wu, Victor Ogunjimi, Mary Ann Sebastian et al.



ECS Membership = Connection

ECS membership connects you to the electrochemical community:

- Facilitate your research and discovery through ECS meetings which convene scientists from around the world;
- Access professional support through your lifetime career:
- Open up mentorship opportunities across the stages of your career;
- Build relationships that nurture partnership, teamwork—and success!

Join ECS! Visit electrochem.org/join



doi:10.1088/1757-899X/1241/1/012021

Temperature dependent pinning efficiency in multilayer and single layer BZO/YBCO nanocomposite films

M Panth^{*1}, V Ogunjimi¹, M A Sebastian^{2,3}, D Zhang⁴, B Gautam¹, J Jian⁴, J Huang⁴, Y Zhang⁴, T Haugan², H Wang⁴, and J Wu¹

¹Department of Physics and Astronomy, the University of Kansas, Lawrence, Kansas 66045, USA

²U.S Air Force Research Laboratory, Aerospace Systems Directorate, WPAFB, OH 45433, USA

³University of Dayton Research Institute, Dayton, OH 45469, USA

Abstract: The BaZrO₃/YBa₂Cu₃O₇ (BZO/YBCO) interface has been found to affect the vortex pinning efficiency of one-dimensional artificial pinning centers (1D-APC) of BZO. A defective BZO/YBCO interface due to a lattice mismatch of ~7.7% has been blamed for the reduced pinning efficiency. Recently, we have shown incorporating Ca_{0.3}Y_{0.7}Ba₂Cu₃O_{7-x} spacer layers in BZO/YBCO nanocomposite film in multilayer (ML) format can lead to a reduced lattice mismatch ~1.4% through the enlargement of lattice constant of YBCO via Ca diffusion and partial Ca/Cu replacement on Cu-O planes. In this work, the effect of this interface engineering on the BZO 1D-APC pinning efficiency is investigated at temperatures of 65-81 K through a comparison between 2 and 6 vol.% BZO/YBCO ML samples with their single-layer (SL) counterparts. An overall higher pinning force (F_p) density has been observed on the ML samples as compared to their SL counterparts. Specifically, the peak value of F_p ($F_{p,max}$) for the 6% BZO/YBCO ML film is about ~ 4 times of that of its SL counterpart at 65 K. In addition, the location of the $F_{p,max}$ (B_{max}) in the ML samples shifts to higher values as a consequence of enhanced pinning. For the 6% BZO/YBCO ML sample, a much smaller "plateau-like" decrease of the B_{max} with increasing temperature was observed, which is in contrast to approximately linear decrease of B_{max} with increasing temperature in the 6% SL film. This result indicates the importance of restoring the BZO/YBCO interface quality for better pinning efficiency of BZO 1D-APCs especially at higher BZO doping concentration.

Keywords: BZO/YBCO interface, pinning efficiency, strain field, lattice mismatch, vortex pinning

1. Introduction:

High temperature superconducting (HTS) wires based on YBa₂Cu₃O₇ (YBCO) coated conductors are a critical element to realize a broad variety of applications including power transmission cables, transformers, fault current limiters, high field magnets, etc. [1-4]. The temperature and field regimes in which these devices are operated are different, ranging in a few to tens of Teslas, depending on specific applications. Improved magnetic vortex pinning via the addition of nanoscale impurity artificial pinning centers (APCs) into the YBCO matrix has provided a viable approach towards achieving high critical current density (*J_c*) at applied magnetic fields and temperatures [5, 6]. Various APCs of different morphologies, including c-axis aligned one-dimensional nanorods (1D-APCs), ab-plane aligned two-dimensional planar defects (2D-APCs), and three-dimensional nanoparticles (3D-APCs) have been reported through the addition of secondary dopants like BaZrO₃ (BZO), BaHfO₃ (BHO), BaSnO₃ (BSO), YBa₂(Nb/Ta)O₆, Y₂O₃, etc. in YBCO (or other rare-earth variation of YBCO) to form APC/YBCO nanocomposites films [7-15].

The self-assembly of the c-axis aligned 1D-APCs in the YBCO matrix via vertical epitaxy is driven by a strain field that originates from the 1D-APC/YBCO interface due to their lattice mismatch at the interface (in the direction of the c-axis of YBCO perpendicular to the film) [8, 16, 17]. In the case of the BZO 1D-APC/YBCO and at the BZO 1D-APC/YBCO interface and hence a tensile strain on the c-axis of YBCO [18]. This leads to a highly defective BZO/YBCO interface for reduction of the interface strain [19]. In contrast, an approximately coherent BHO 1D-APC/YBCO interface with a

⁴School of Materials Engineering, Purdue University, West Lafayette, IN 47907, USA

^{*}Corresponding author E-mails: panthm@ku.edu, jwu@ku.edu

Content from this work may be used under the terms of the Creative Commons Attribution 3.0 licence. Any further distribution of this work must maintain attribution to the author(s) and the title of the work, journal citation and DOI.

1241 (2022) 012021

doi:10.1088/1757-899X/1241/1/012021

much reduced interface defect concentration was observed and attributed to a smaller lattice mismatch of ~6.7% and more adaptive elastic properties of BHO [13]. The higher pinning efficiency of BHO 1D-APCs, as reflected in the more than twice higher maximum pinning force density $F_{p,max}$ ~182 GNm⁻³ at 65 K than that of BZO 1D-APCs, suggests a close correlation between the pinning efficiency of 1D-APCs and the 1D-APC/YBCO interface quality [13]. Among others, BZO 1D-APCs have been intensively studied after the pioneering work by Driscoll et al [7]. Despite a large BZO/YBCO lattice mismatch, BZO 1D-APCs can form at fairly high concentrations proportional linearly to the BZO doping approximately up to 10 vol.%, which is important to enhance pinning at high applied magnetic fields [20-26]. In contrast, the concentration of the BHO 1D-APCs exhibits a nonlinear dependence on the BHO doping and could not seem to be further increased above BHO doping of 4-5 vol.% [12, 13, 27]. In fact, when BHO 1D-APCs form coherent interfaces with YBCO, the accommodation of the BHO and YBCO lattices leads to not only a large strain that hampers formation of high concentration BHO 1D-APCs, but also degrades T_c of the BHO/YBCO nanocomposite films. At 6 vol.% BHO doping, T_c decreases to ~78 K, which results in much reduced J_c in the temperature range of 65-77 K [13].

Considering the advantages of BZO in generating high-concentration 1D-APCs in BZO/YBCO nanocomposite films, repairing the BZO/YBCO interface may recover the pinning efficiency of the BZO 1D-APCs. In a recent exploration, we have developed a multilayer (ML) approach by inserting two Ca_{0.3}Y_{0.7}Ba₂Cu₃O_{7-x} (CaY-123) spacer layers in BZO/YBCO nanocomposite film for improving the BZO/YBCO interface after BZO 1D-APCs form in BZO/YBCO nanocomposite films. In the ML films, Ca from the spacer layers can diffuse dynamically during the film growth to YBCO layers. While replacements of Y, Ba and Cu with Ca are all possible, the Ca/Cu replacement is most favorable, as compared to the other two options on tensile strained YBCO lattice (in c-axis due to formation of BZO 1D-APCs). This is because Ca/Cu replacement can lead to elongated c-axis lattice constant of YBCO up to 1.24 nm when the Cu cations of smaller size (by 30%) on the Cu-O planes are partially replaced with larger Ca cations. This prevents formation of interface defects, such as dislocations, and leads to a coherent BZO/YBCO interface owing to the reduced lattice mismatch up to ~1.4%. Considerably enhanced pinning efficiency of BZO 1D-APCs has been observed [28]. It should be noted that the Ca diffusion and Ca/Cu replacement occur dynamically during the growth of the BZO 1D-APCs with a minimum impact on the nucleation (or the concentration) of the BZO 1D-APCs. In this paper, a systematic study of the pinning efficiency of the BZO 1D-APCs in 2% and 6% BZO/YBCO ML samples as a function of temperature in the range of 65-81 K is presented using single-layer BZO/YBCO (SL) samples as a reference. Significant J_c enhancement is obtained in the temperature range of 65-81 K as illustrated in the overall higher pinning force density (F_p) and reduced temperature dependence of pinning in ML samples as compared to their SL counterparts', which can be attributed to the formation of coherent BZO 1D-APC/YBCO interface and thereby restoration of the pristine pinning efficiency of the BZO 1D-APCs.

2. Experimental

In this work, 2 and 6 vol.% BZO doped YBCO nanocomposite films were deposited on (100) SrTiO₃ (STO) single crystal substrates. One set of samples were made as reference samples, which included single-layered YBCO films doped with 2 and 6 vol.% BZO (BZO/YBCO-SL). These samples are referred as 2% SL and 6% SL, respectively, in the rest of the paper. The other set of samples is the same except incorporation of two calcium containing Ca_{0.3}Y_{0.7}Ba₂Cu₃O_{7-x} (CaY-123) spacer layers inserted in each BZO doped YBCO nanocomposite film. These samples have a multilayer structure with three ~50 nm thick BZO doped YBCO layers separated by two alternating ~10 nm thick spacer layers and will be regarded as BZO/YBCO-ML and which are denoted by 2% ML and 6% ML in rest of the paper. All samples were made using pulsed laser deposition (PLD) technique. A KrF excimer laser was employed for PLD at the laser wavelength ~248 nm, with a pulse energy ~450 mJ. The optimal PLD repetition rates were 8 Hz and 2 Hz for BZO/YBCO and the CaY-123 spacer layers respectively. During the sample deposition, the oxygen pressure was maintained at ~300 mTorr whereas the sample temperature was set at 825°C [29]. After the PLD deposition, the films were annealed at 500 °C in 1 atmospheric oxygen pressure for 30 minutes. The details of the BZO/YBCO SL film fabrication have been reported previously [27, 30, 31]. The film thicknesses were measured using a Tencor P-16 profilometer. The thicknesses of SL and ML samples are around 150 nm and 170 nm respectively. Crystallinity and lattice

parameters were determined by x-ray diffraction (XRD) utilizing a Bruker D8 Discover diffractometer. In both SL and ML samples, c-axis aligned BZO 1D-APCs have been confirmed using transmission electron microscopy [28] with a diameter ~5 nm and comparable concentrations at the given BZO doping.

In order to study the electrical transport properties, two parallel microbridges with length of 500 μ m and width of 20 or 40 μ m were patterned on each film using standard photolithography. The details of the patterning and sample wiring for the transport measurement can be found in our previous works [27, 30, 31]. Briefly, Ag contact pads of ~ 120 nm in thickness were deposited through a shadow mask using DC magnetron sputtering at the deposition rate of approximately 0.07 nm/second under the argon pressure of 30 mTorr. The electrical connection to the microbridges were made by attaching platinum wires of 50 μ m in diameter on Ag pads using Indium. The $J_c(B)$ measurement were taken at $\theta = 0^{\circ}$ (B/c-axis) and at temperatures of 65-81 K. Quantum Design Ever-Cool II Physical Property Measurement System equipped with a 9 T magnet was used for the electrical transport measurement. Standard four-probe technique was used in the measurement of the transport properties including resistance-temperature (R-T) curves from which T_c can be determined, and $J_c(B)$ curves. The J_c values were determined by applying a standard criterion of 1 μ V/cm. The pinning force density (F_p) was calculated from the equation $F_p = J_c \times B$. The maximum pinning force density ($F_{p,max}$) and its location (B_{max}) were determined from the $F_p(B)$ curves.

3. Results

Figure 1a and 1b compare the XRD θ -2 θ spectra of the 2% and 6% SL and ML films. The SL films are denoted by black and ML in red respectively. The appearance of the YBCO (001) peaks (#) indicates the c-axis orientation of the BZO/YBCO nanocomposite films on the (100) STO substrates (+). Additionally, both SL and ML spectra show the major BZO (001) peaks at $2\theta \sim 46.5^{\circ}$. The c-lattice constants estimated from the YBCO (001) peaks for the 2% and 6% SL films are 11.74 Å and 11.81 Å, respectively. The larger lattice constant in the 6% SL film confirms the increased tensile strain with increased BZO doping most probably attributed to the increased strain field overlap at higher BZO doping [16, 32, 33]. Meanwhile the same c-lattice constants of 11.76 Å is observed on both the 2% and 6% ML films. This may be attributed to the combined effects from interfacial strain and partial Ca/Cu replacement as shown in our recent works. Basically, the replacement is mostly happening around the BZO/YBCO interface where maximum tensile strained occurs. This has been confirmed via High resolution transmission electron microscopy images with the elongated c-axis lattice constant of YBCO up to 1.24 nm as described in the previous work [28]. A coherent BZO/YBCO interface was formed owing to the reduced lattice mismatch up to ~1.4%.

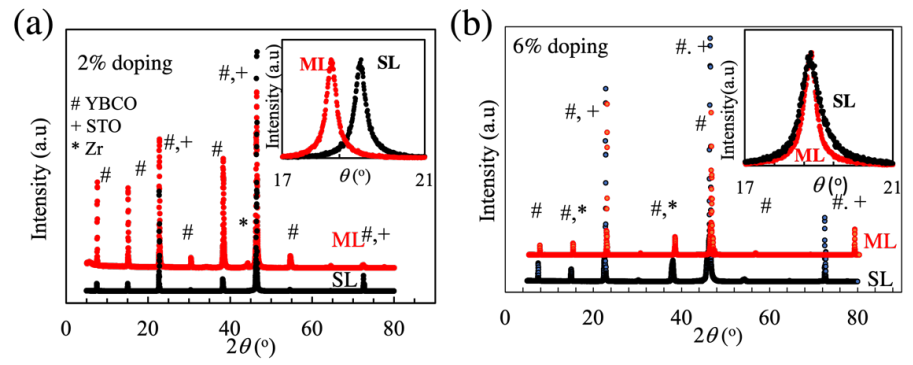


Figure 1: X-ray diffraction. (a) θ -2 θ scans taken on 2% SL (black) and 2% ML (red) with the inset showing rocking curves of the YBCO (005) peak for the 2% SL (black) and ML (black) films. (b) θ -2 θ scans taken on 6% SL (black) and 6% ML (red) with the inset showing rocking curves of the YBCO (005) peak for the 6% SL (black) and ML (red) films. The spectra were generated using Cu-k α radiation of wavelength 1.54 Å. The symbols #, + and * represent the YBCO (001), STO substrate (100) and major BZO (001) peaks respectively.

This Ca/Cu replacement on YBCO's Cu-O planes resulting in strain reduction is evidenced in the microstrain evaluation in XRD data shown in figure 1. In the 6% ML film, the c-lattice constant decreases as compared to its SL counterparts. This can be explained via higher reduction of microstrain as revealed in its FWHM values evaluated from (005) YBCO rocking curves. These are shown in the inset of figure 1a and 1b for 2% and 6% SL and ML (SL as black and ML as red curves) sample respectively. This has been confirmed from the smaller full width at a half maximum (FWHM) of YBCO (005) rocking curves on the 2% and 6% ML samples. The FWHM values for the 2% SL and ML samples are 0.35° and 0.32° respectively, which correspond to ~ 10% reduction in the microstrain in the latter as opposed to the former. In the 6% SL and ML samples, the FWHM values are 0.59° and 0.38° respectively. This means that a reduction of 35% of microstrain is obtained in the 6% ML film as compared to its counterpart. In addition, the c-lattice constant of 6% ML sample is the same as that of the 2% ML sample. This result therefore suggests the benefit of the ML approach is more significant in BZO/YBCO nanocomposites with higher BZO doping concentrations, in which strain field overlap is more significant and the impact on the nanocomposite performance is more severe.

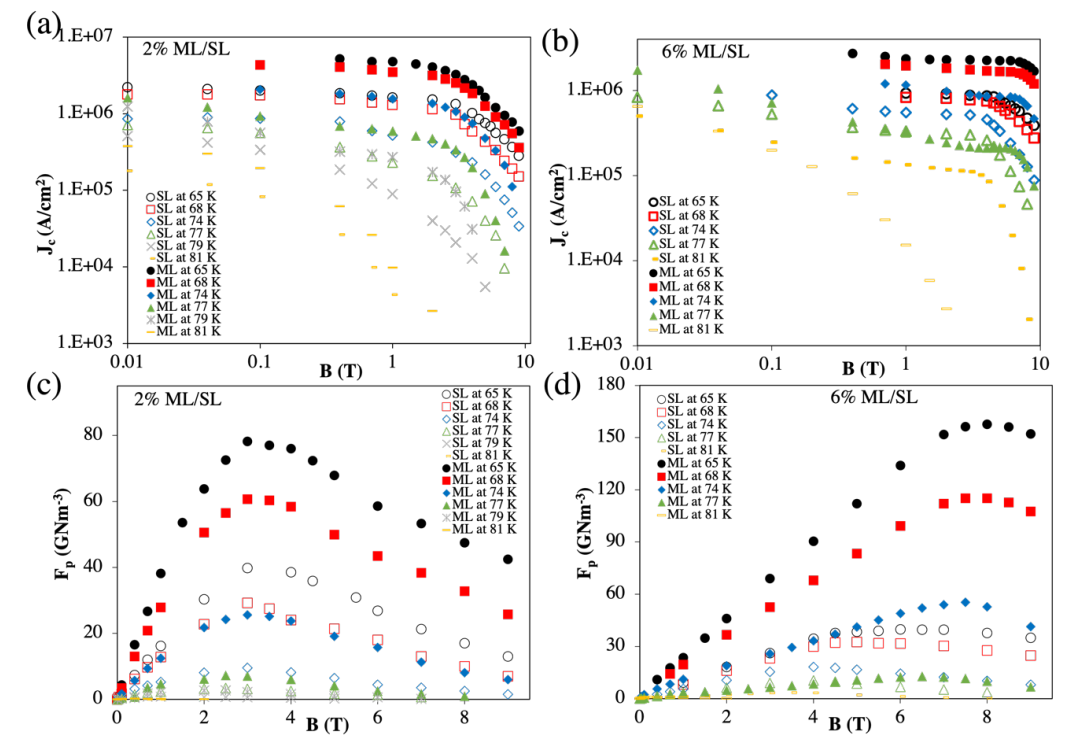


Figure 2: (a) Comparisons of $J_c(B)$ curves of the 2% SL with 2% ML nanocomposite films at B//c. (b) Comparisons of $J_c(B)$ curves of the 6% SL with 6% ML nanocomposite films at B//c. $F_p(B)$ plots at different temperature for (c) 2% SL and ML films (d) 6% SL and ML films.

The T_c values are determined to be 89.2 K, 87.5 K from the R-T curve measurement on the 2% SL and ML samples. Similarly, the T_c values of 86.9 K and 84.0 K, respectively, were observed on the 6% SL and ML samples. The slightly reduced T_c values in the ML samples indicates a minor Ca diffusion is happening in the YBCO matrix due to the Ca diffusion from the CaY-123 spacers [34, 35]. Figure 2a compares the $J_c(B)$ curves of the 2% SL and ML films at B//c in the field range of 0-9 T and temperature range of 65-81 K. The ML samples exhibit overall higher J_c values in high field range despite a lower T_c (by ~1.0 K) in the ML samples. For example, at 65 K, a J_c enhancement of 2.9, 2.4, 2.1, and 2.1 times is observed on the 2% ML samples at 1 T, 3 T, 5T and 9 T respectively over the 2% SL samples. At 77 K, the J_c enhancement factor of 2.5, 3.1 and 2.2 is observed at 1 T, 3 T and 5 T respectively. Similarly, at 81 K, the 2% ML sample has 1.7, 2.2 times higher J_c at self-field and at 1 T. Furthermore, the $J_c(B)$ curve for the 2% ML sample exhibits much reduced B-field susceptibility as compared with the 2% SL

sample at all temperature study conducted. These results suggest the benefits of ML approach in enhancing the J_c via restoration of pristine pinning efficiency of BZO 1D-APCs. Figure 2b compares the $J_c(B)$ curves of the 6% SL and ML films at B//c in the field range of 0-9 T and temperature range of 65-81 K. A similar trend of enhanced pinning has been observed in the 6% ML sample as compared to its SL counterpart. At 65 K, the ML samples show J_c enhancement factors of 2.5, 2.6, 2.9, and 4.3 times over its SL counterparts at 1 T, 3 T, 5 T and 9 T respectively. At 77 K, ML sample has 0.95, 0.72, and 1.2 times higher J_c than SL counterparts at 1 T, 3 T and 5 T respectively. Similarly, at self-field and 1 T, J_c enhancement of 1.6 and 0.11 is observed for ML samples at 81 K. It should be noted that the higher J_c values for the 6% ML sample were observed in the entire field range at almost all temperatures. It is seen from $J_c(B)$ plots, magnetic field susceptibility for 2% ML sample is higher than 6% ML samples. This suggest that a larger number of BZO 1D-APCs are efficient for pinning in the 6% ML sample, which is expected from the higher concentration of BZO doping in BZO/YBCO nanocomposite. In addition, the $J_c(B)$ enhancement increases with the applied B fields. For example, at a temperature of 65 K and 68 K, the J_c value for the 6% ML sample is about 4.3 times of that of the 6% SL counterparts at 9 T, which is in contrast to ~2.1 in the 2% case at the same condition.

The enhanced $J_c(B)$ leads to an enhanced $F_p(B)$ in the 2% ML sample in the entire temperature range of measurements as shown in figure 2c. The $F_p(B)$ curves are of a characteristic bell shape for both SL and ML samples and the peak value of $F_p(F_{pmax})$ locates at B_{max} . For the entire temperature and field range higher F_p values can be observed for ML sample. At 65 K, the F_{pmax} 's for the ML and SL samples locate almost at the same locations of $B_{\text{max}} \sim 3.0 \text{ T}$ despite an enhanced F_{pmax} value by approximately 96% from \sim 39.8 GN/m³ for the 2% SL sample to \sim 78.1 GN/m³ for the 2% ML sample. At 1 T, 5 T and 9 T, an enhancement factor of 2.3, 2.1, and 3.2 times has been observed on the ML sample over its SL counterpart's. At 77 K, approximately ~2 times higher F_p at 1 T, 3 T and 5 T observed for 2% ML sample as compared with SL counterparts. In comparison with 2% case, the 6% ML sample shows much more enhanced F_p which is shown in figure 2d. At 65 K and fields of 1 T, 5 T, and 9 T ML sample has F_p values 2.5, 2.9 and 4.1 times of SL counterparts respectively. In addition, an overall higher B_{max} values can be seen in 6% ML sample as compared to the 6% SL sample. At 65 K, the $B_{max} \sim 8$ T is approximately 33% higher than that of the 6% SL sample. At 77 K, F_p values are comparable and little better for ML samples compared to SL counterparts. For example, F_p enhancement of 0.95, 0.72 and 1.2 at 1 T, 3 T and 5 T respectively observed at 77 K. The F_p 's enhancement are consistent with the J_c 's enhancement observed in figure 2a and 2b.

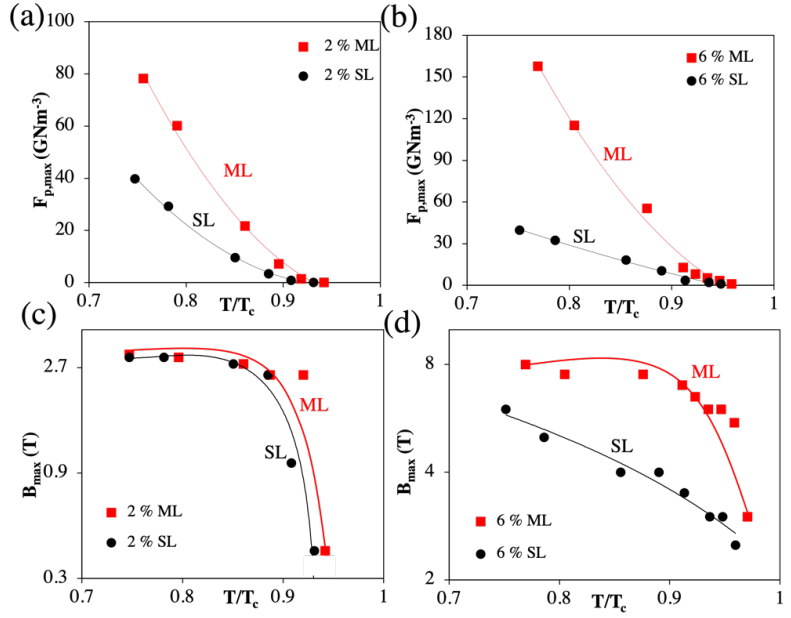


Figure 3: Pinning force density ($F_{p,max}$) as a function of reduced temperature (T/T_c) plots for (a) 2% SL and ML sample (b) 6% ML and SL sample. B_{max} vs T/T_c plots for (c) 2% SL and ML sample (d) 6% ML and SL sample.

IOP Conf. Series: Materials Science and Engineering

1241 (2022) 012021

doi:10.1088/1757-899X/1241/1/012021

Figure 3a and 3b compare the $F_{P,max}$ values as a function of reduced temperature (T/T_c) for the 2% and 6% SL and ML samples, respectively. Overall, high $F_{p,max}$ values are observed on ML samples as compared to their SL counterparts'. At $T/T_c = 0.755$, the $F_{p,max}$ values ais 78.1 GNm⁻³, and at $T/T_c = 0.769$, $F_{p,max}$ values is 157.7 GNm⁻³ for 2% and 6% ML samples, which are 1.9 and 3.9 times of their SL counterparts'. At $T/T_c = 0.91$, the ratios between $F_{p,max}$ values of ML and SL samples are 1.6 and 3.6 for 2% and 6% samples. Although the SL and ML samples exhibit a similar temperature dependence of $F_{P,max}$, the higher $F_{P,max}$ values in the ML samples imply an extension of the temperature range for applications of the BZO/YBCO nanocomposites.

Figure 3c and 3d compare the B_{max} as a function of T/T_c for the 2% and 6% samples, respectively. At the lower BZO doping of 2 vol.%, the B_{max} values for the SL and ML samples are comparable in the lower T/T_c range up to ~0.85, while higher B_{max} values are observed in the ML sample. This illustrates the benefit of the BZO/YBCO interface engineering using the multilayer approach. Specifically, the removal of the defective YBCO interfacial layer would lead to reduced degradation of the T_c value at the interface. A sharper BZO/YBCO interface is critical to the pinning efficiency of BZO 1D-APCs [36]. Specifically, the higher B_{max} values in the 2% ML sample implies more BZO 1D-APCs remain efficient at elevated temperatures. A similar but more dramatic trend can be observed in 6 vol.% samples. In fact, the B_{max} vs T/T_c curves for SL and ML samples differ qualitatively, besides much higher B_{max} values for the ML sample over the entire range of T/T_c . At $T/T_c \sim 0.76$, the $B_{max} \sim 8$ T for the ML sample is 1.3 times of that for the SL sample. At $T/T_c \sim 0.95$, this ratio is increased to 2.2. In contrast to the approximately linear decreases of the B_{max} vs T/T_c in the SL sample, a more or less plateau can be seen in that for the ML sample at lower T/T_c , followed by a sharp decrease of the B_{max} when approaching $T/T_c = 1$. For example, in 2% ML, B_{max} drop sharply to 0.4 T at $T/T_c \sim 1$ from B_{max} of 2.5 T when T/T_c equals to 0.91. Similarly in 6% ML film, B_{max} drops to 3 T at $T/T_c \sim 1$ from 5.5 T at $T/T_c \sim 0.95$. This observation suggests that the BZO 1D-APCs lose their pinning efficiency at elevated temperatures in SL samples, while they remain efficient pins in a wider temperature range in the ML sample. In contrast, the more dramatic enhancement of the pinning in the 6% ML sample is not surprising considering the expected benefits of improved BZO/YBCO interface and reduced strain field overlap at high concentration of the BZO 1D-APCs.

4. Conclusions

A newly developed ML scheme by inserting two ~10 nm thick CaY-123 spacer layers in 2% and 6% BZO 1D-APCs/YBCO nanocomposite films has shown to enhance the pinning efficiency of BZO 1D-APCs by reducing the BZO/YBCO interface lattice mismatch and hence interfacial defect concentration. Significant J_c enhancement has been observed on ML samples as compared to their SL counterparts in the temperature range of 65-81 K. For example, a J_c enhancement of 4.3 times in 6% ML film has been observed at 65 K and at magnetic field of 9 T in comparison with 6% SL counterparts. The overall J_c enhancement has led to enhanced $F_{p,max}$ value by approximately 96% for the 2% ML and 296% for the 6% ML samples, respectively. The pinning enhancement in the ML samples is also illustrated in their higher B_{max} values in the temperature range of 65-81 K. Furthermore, a qualitatively different temperature dependence of B_{max} has been observed on 6% ML sample as compared to the 6% SL one. Specifically, a much smaller decrease of the B_{max} values with increasing temperature has been observed in the ML sample, suggesting that the majority of BZO 1D-APCs remain efficient in pinning at temperatures close to T_c . This result indicates the importance of the BZO/YBCO interface on pinning efficiency of BZO 1D-APCs.

5. References

- [1] Alecu G Crystal structures of some high-temperature superconductors Romanian Reports in Physics 2004 56(3) p 404-412.
- [2] Mourachkine A Room-temperature superconductivity 2004 Cambridge Int Science Publishing.
- [3] Obradors X and T Puig Coated conductors for power applications materials challenges Superconductor Science and Technology 2014 27(4) p 044003.
- [4] Kalsi S S Applications of high temperature superconductors to electric power equipment 2011 John Wiley & Sons.

doi:10.1088/1757-899X/1241/1/012021

- [5] Matsumoto K and P Mele Artificial pinning center technology to enhance vortex pinning in YBCO coated conductors. Superconductor Science and Technology 2009 23(1) p 014001.
- [6] Matsumoto K et al Enhancement of critical current density of YBCO films by introduction of artificial pinning centers due to the distributed nano-scaled Y₂O₃ islands on substrates Physica C Superconductivity 2004 412 p 1267-1271.
- [7] MacManus-Driscoll J et al Strongly enhanced current densities in superconducting coated conductors of YBa₂Cu₃O_{7-x+} BaZrO₃ Nature materials 2004 3(7) p 439-443.
- [8] Wu J and J Shi Interactive modeling-synthesis-characterization approach towards controllable in situ self-assembly of artificial pinning centers in RE-123 films Superconductor Science and Technology 2017 30(10) p 103002.
- [9] Miura S et al Strongly enhanced irreversibility field and flux pinning force density in SmBa₂Cu₃O y-coated conductors with well-aligned BaHfO₃ nanorods Applied Physics Express 2017 10(10) p 103101.
- [10] Chen, S., et al., Generating mixed morphology BaZrO₃ artificial pinning centers for strong and isotropic pinning in BaZrO₃–Y₂O₃ double-doped YBCO thin films. Superconductor Science and Technology, 2017. 30(12): p. 125011.
- [11] Mele P et al *Ultra-high flux pinning properties of BaMO₃-doped YBa*₂ Cu_3O_{7-x} thin films (M=Zr, Sn) Superconductor Science and Technology 2008 21(3) p 032002.
- [12] Gautam B et al Transformational dynamics of BZO and BHO nanorods imposed by Y₂O₃ nanoparticles for improved isotropic pinning in YBa₂Cu₃O_{7-δ} thin films AIP Advances 2017 7(7) p 075308.
- [13] Gautam B et al *Probing the effect of interface on vortex pinning efficiency of one-dimensional* BaZrO₃ and BaHfO₃ artificial pinning centers in YBa₂Cu₃O_{7-x} thin films Applied Physics Letters 2018 113(21) p 212602.
- [14] Wu J, B Gautam, and V Ogunjimi Pinning Efficiency of Artificial Pinning Centers in Superconductor Nanocomposite Films in Superconductivity 2020 Springer p 29-52.
- [15] Ogunjimi V et al *The angular range of effective pinning by one-dimensional artificial pinning centers in BaZrO₃/YBa₂Cu₃O_{7-x} nanocomposite films AIP Advances 2019 9(8) p 085110.*
- [16] Horide T et al Structural evolution induced by interfacial lattice mismatch in self-organized YBa₂Cu₃O_{7-δ} nanocomposite film ACS nano 2017 11(2) p 1780-1788.
- [17] Wu J Z et al *The effect of lattice strain on the diameter of BaZrO₃ nanorods in epitaxial* $YBa_2Cu_3O_{7-\delta}$ *films* Superconductor Science and Technology 2014 27(4) p 044010.
- [18] File P D Joint Committee on Powder Diffraction Standards (JCPDS) ASTM, Philadelphia PA
- [19] Cantoni C et al Strain-driven oxygen deficiency in self-assembled, nanostructured, composite oxide films Acs Nano 2011 5(6) p 4783-4789.
- [20] Wee S H et al Engineering nanocolumnar defect configurations for optimized vortex pinning in high temperature superconducting nanocomposite wires Scientific reports 2013 3 p 2310.
- [21] Horide T et al *Influence of matching field on critical current density and irreversibility temperature in YBa*₂Cu₃O₇ films with BaMO3 (M= Zr, Sn, Hf) nanorods. Applied Physics Letters 2016 108(8) p 082601.
- [22] Horide T et al *Elastic strain evolution in nanocomposite structure of YBa*₂*Cu*₃*O*₇+ *BaZrO*₃ superconducting films Japanese Journal of Applied Physics 2014 53(8) p 083101.
- [23] Xu A et al Strongly enhanced vortex pinning from 4 to 77 K in magnetic fields up to 31 T in 15 mol.% Zr-added (Gd, Y)-Ba-Cu-O superconducting tapes. Apl Materials 2014 2(4) p 046111.
- [24] Goyal A et al Irradiation-free, columnar defects comprised of self-assembled nanodots and nanorods resulting in strongly enhanced flux-pinning in YBa₂Cu₃O_{7-δ} films Superconductor Science and Technology 2005 18(11) p 1533.
- [25] Peurla M et al Effects of nanocrystalline target and columnar defects on flux pinning in pure and BaZrO₃-doped YBa₂Cu₃O_{6+ x} films in fields up to 30 T Physical Review B 2007 75(18) p 184524.
- [26] Wu J et al *Pinning efficiency of one-dimensional artificial pinning centers in YBa*₂*Cu*₃*O*_{7-x} thin films IEEE Transactions on Applied Superconductivity 2019 29(5) p 1-5.

- [27] Sebastian M A P et al Study of the flux pinning landscape of YBCO thin films with single and mixed phase additions BaMO₃+ Z: M= Hf, Sn, Zr and Z= Y₂O₃, Y211 IEEE Transactions on Applied Superconductivity 2017 27(4) p 1-5.
- [28] Ogunjimi V et al Enhancing Magnetic Pinning by BaZrO₃ Nanorods Forming Coherent Interface by Strain-Directed Ca-doping in YBa₂Cu₃O_{7-x} Nanocomposite Films Superconductor Science and Technology 2021.
- [29] Baca F J et al Interactive growth effects of rare-earth nanoparticles on nanorod formation in $YBa_2Cu_3O_x$ thin films Advanced Functional Materials 2013 23(38) p 4826-4831.
- [30] Chen S et al Enhancement of isotropic pinning force in YBCO films with $BaZrO_3$ nanorods and Y_2O_3 nanoparticles IEEE Trans. Appl. Supercond 2017 27(4) p 4-8.
- [31] Wang X et al Eliminating thickness dependence of critical current density in YBa₂Cu₃O_{7-x} films with aligned BaZrO₃ nanorods Journal of Applied Physics 2010 108(11) p 113911.
- [32] Khan M Z et al Enhanced flux pinning isotropy by tuned nanosized defect network in superconducting YBa₂Cu₃O_{6+ x} films Scientific reports 2019 9(1) p 1-12.
- [33] Samoilenkov S et al Anisotropic strain of BaZrO₃, BaCeO₃ and Y₂O₃ nanoinclusions in a YBa₂Cu₃O_{7-x} epitaxial film matrix and its relation to the oxygen content of the superconductor Superconductor Science and Technology 2011 24(5) p 055003.
- [34] Hammerl G et al Enhanced supercurrent density in polycrystalline YBa₂Cu₃O_{7-δ} at 77 K from calcium doping of grain boundaries Nature 2000 407(6801) p 162.
- [35] Schmehl A et al Doping-induced enhancement of the critical currents of grain boundaries in $YBa_2Cu_3O_{7-\delta}$ EPL (Europhysics Letters) 1999 47(1) p 110.
- [36] Blatter G et al *Vortices in high-temperature superconductors*. Reviews of modern physics 1994 66(4) p 1125.

Acknowledgement

This research was supported in part by NSF contracts Nos: NSF-DMR-1508494 and 1909292 and NSF-ECCS-1809293, the AFRL Aerospace Systems Directorate, the Air Force Office of Scientific Research (AFOSR) LRIR #14RQO8COR and LRIR #18RQCOR100. D.Z. and H.W. acknowledge the support from the U.S. National Science Foundation for the high-resolution STEM effort at Purdue University (DMR-1565822 and DMR-2016453).